Realistic Time-Domain Simulations of Arc Faults in Low-Voltage Installations

Matija Varga
Integrated Sensor Systems
ABB Corporate Research
Baden-Dättwil, Switzerland
ORCID: 0000-0003-1185-7192

Yannick Maret
Integrated Sensor Systems
ABB Corporate Research
Baden-Dättwil, Switzerland

Stefano Maranò
Integrated Sensor Systems
ABB Corporate Research
Baden-Dättwil, Switzerland

Luca Ghezzi
Electrification Products
ABB S.p.A.
Vittuone, Italy

Agostino Butti
Electrification Products
ABB S.p.A.
Vittuone, Italy

***Abstract*—Electric arc faults that appear in home installations pose a significant safety hazard that may result in an outbreak of fire. Such events can be prevented using an arc fault detection device (AFDD) that interrupts the electrical circuit upon detecting an arcing event. In this work, we propose a realistic model of an arc fault for electrical simulations of low-voltage installations. We model an arc fault as a circuit component whose parameters dynamically change to account for the stochastic behaviour of electric arcs. The model uses a black-box representation that consists of a set of mathematical equations that link current and voltage. The proposed model goes beyond the state of the art by dynamically adapting the arc parameters after each current zero crossing. The parameters and their statistical distributions are extracted from laboratory measurements using optimization methods. In addition to that, we implement a noise source within the arc model with power spectral density that follows 1/f law. Power spectral density is extracted from an actual noise measurement. Transient behaviour of the modelled arc fault is implemented in an analogue and mixed signal simulation engine based on VHDL-AMS. The developed component can be used as a part of more complete electric installation simulation.**

Keywords—arc simulation, arc fault

I. Introduction

Arc faults in home installations can appear due to different reasons: 1) damaged isolation between line, neutral and ground wires, 2) partially interrupted line or neutral wires, 3) poor electrical contacts, or 4) a faulty electrical device. The latter may include reasons 1)-3) and may be difficult to predict. Arc faults may occur in parallel or in series with loads. In latter case, the load impedance limits the fault current. Series arc faults pose a greater safety threat because they typically occur at current levels that are below the tripping levels of conventional circuit breakers (e.g. overcurrent and overvoltage protection devices).

An arc fault detection device (AFDD) or an arc fault circuit interrupter (AFCI) is used to continuously analyse the current and/or voltage in an electrical installation and interrupt the circuit upon detecting an arc fault. During product development, AFDDs are tested in a laboratory setting as well as in real-life scenarios. On the one hand, such tests are crucial for design engineers that want to integrate novel technological solutions in their products. On the other hand, running tests can be costly and time consuming, which strongly impacts the time-to-market of a new product. Having a virtual prototyping tool could fast forward the testing and prototyping processes, thus reducing the time-to-market of new products.

Virtual prototyping tool for AFDDs determines the currents and voltages in branches and nodes of the simulated electric installation. Therefore, an arc fault should be modelled as one of the circuit components with a known impedance. There are different models that use black-box approach to describe the impedance of the arc. Black-box models describe the relation between the arc current and voltage while implicitly including other physical parameters.

Early black-box models that were introduced by Cassie [1] and Mayr [2] are well suited for arcs that appear during opening and closing of contacts. Over the years there have been different variations and improvements of the latter models. Improvements include introducing additional non-physical parameters to more accurately match the measured data. Nevertheless, Schavemaker et al. and Orama et al. showed improved Mayr models with successful fitting in certain applications [3], [4]. Habedank model combines conductance of Cassie and Mayr model by connecting them in parallel, which results in a model that can more accurately model low (Mayr model's feature) and high currents (Cassie model's feature) during arcing [5].

As expected, previously described models do not accurately model all stages of a typical arc fault in home installations: 1) carbonization, 2) ignition, and 3) extinction. Classical [1], [2], [6] as well as more elaborated [7] short circuit arc models fail to adequately describe arc faults, because currents are different than those in (series) arc faults (kA vs. A). In addition to that, short circuit arcs take place in circuit breakers while arc faults appear in cables. A model by Andrea et al. [8] models all three phases of an arc fault and serves as a starting point of this work. In that model, a static characteristic, i.e. the relation between current and voltage, is obtained by fitting a mathematical function to the measured data. Furthermore, that model has the lowest error between measured and simulated data when compared to Mayr and Schavemaker model [9].

Here, we present an arc fault model, which is a key component of our virtual prototyping tool. We go beyond the state of the art by describing the stochastic behaviour of an arc fault. We extract the parameters of the model from different laboratory measurements and analyse their statistical features. In addition to that, we show correlations between arc fault parameters and different features that can be observed in an arc fault waveform. Finally, we characterize the high

frequency component (>200 kHz) of the arc fault signal and jointly simulate both the high and low frequency behaviour in a transient simulation.

Chapter II introduces the model that is used in this work, measurements of arc faults, identification of arc fault parameters from measurements, and extraction of physical features from measured arc fault waveforms. Chapter III shows how different values of arc fault parameters influence and correlate with the arc fault waveform and how they are distributed. Finally, a transient simulation of arc fault with 1/f noise is carried out. Chapter IV discusses the results and some limitations of the approach. We finally conclude in Chapter V.

II. Methods

A. Mathematical arc fault model

We base our model on [8] and refer to it as a mathematical arc fault model. The central part of the model is the static characteristic (1), which is parameterized by r, β, and α as

$$v_{arc} = \frac{\alpha r i_{arc}}{\arctan(\beta i_{arc}) i_{arc} r + \alpha}. \quad (1)$$

The parameter r in the numerator of (1) governs the behaviour of an arc fault near zero current, the denominator being dominated by α in this condition. In that region, the conduction occurs in the carbonised material of the cable, thus the arc is not ignited. The asymptotic behaviour of the static characteristic determines the voltage of an arc fault at large currents. For higher i_{arc}, v_{arc} converges to α. The parameter β controls the transition between the high current region (arc ignited; low resistance) and the low current region (arc extinguished; high resistance).

The static characteristic alone is not sufficient to simulate the current and voltage of an arc. It is necessary to introduce dynamic equations that model the inertia in the system (e.g. heating and cooling of the surrounding material). For this purpose, the model also includes dynamic equations

$$v_{arc}(t_0 + dt) = v_{arc}(t_0) + \tau \frac{dv_{arc}(t)}{dt}\Big|_{t_0}, \quad (2)$$

$$i_{arc}(t_0 + dt) = i_{arc}(t_0) + \tau \frac{di_{arc}(t)}{dt}\Big|_{t_0}, \quad (3)$$

where τ is the arc time constant.

With static and dynamic equations in place, we can connect the arc model with other circuit components.

B. Arc fault measurements

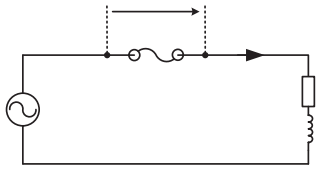

Fig. 1. Schematic of the measurement setup. AF stands for arc fault.

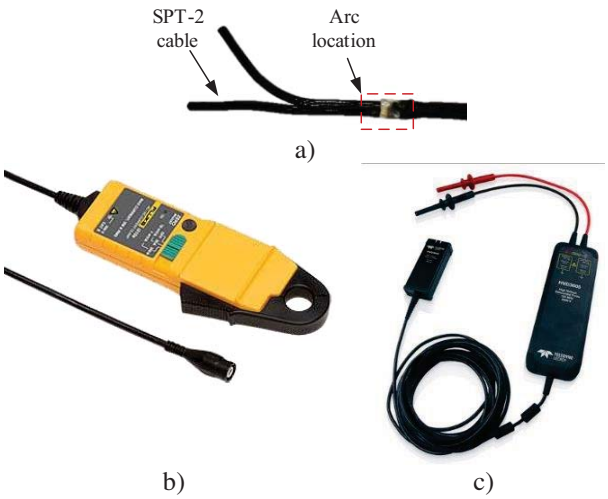

Fig. 2. a) SPT-2 cable test sample. b) Arc current probe Fluke i310s. c) Arc voltage probe LeCroy HDV3106.

Fig. 1 shows a schematic of the measurement setup, which consists of a signal generator v_g, an arc fault (AF), a resistive load R and an inductive load L, which represents the inductance of components in the circuit. Standard power line voltage (230 V_{rms} at 50Hz) is used as a signal generator and the AF test sample is a SPT-2 cable, which consists of two wires – line and neutral. A small portion of line wire is cut, and a cellulose-based tape is wrapped around the incision (Fig. 2a). The test sample is carbonised by first applying a voltage of several kilovolts. The carbonisation is sufficient when the arc can be subsequently ignited under standard power line voltage level. The resistance of that carbonised material is referred to as carbonised path resistance r_{carb}.

Arc fault current is measured using a battery-powered current probe with a bandwidth from 0-20 kHz and the sensitivity of 10mV/A (Fig. 2b). Arc faults are created at currents of 2.5 A_{rms}, 5 A_{rms}, 10 A_{rms}, and 13 A_{rms}. The voltage across the AF is measured using a differential probe (Fig. 2c). Each sample is exposed to up to 3 bursts of power line voltage and one current level. In total, we record data from 21 experiments with 200 ms arcing per experiment. High frequency measurements of voltage noise are conducted using a custom high pass filter and an optically isolated voltage probe (LeCroy HVFO103).

C. Identification of mathematical parameters

We first segment the measured AF voltage and current signals into half-cycles by detecting the zero-crossing time instants of the AF voltage. We define the half-cycle segments as $v_{arc}(t,i)$ and $i_{arc}(t,i)$ for $t \in [t_i, t_{i+1}]$, where the t_i are the detected zero-crossing time instants.

Let us define a function

$$[\tilde{v}_{arc}(t) \quad \tilde{\imath}_{arc}(t)]^T := \boldsymbol{f_{sim}}(t, \alpha, \beta, r, \tau, \boldsymbol{p_{cir}}), \quad (4)$$

that simulates the time evolution of the arc voltage $\tilde{v}_{arc}(t)$ and current $\tilde{\imath}_{arc}(t)$ for the electric circuit depicted in Fig. 1. The function is parametrised by the arc parameters (α, β, r, and τ) and the electric circuit parameters $\boldsymbol{p_{cir}} = [R \quad L]^T$. The function is implemented as reported in [8]. In the following we assume that the circuit parameters $\boldsymbol{p_{cir}}$ are known (e.g. directly measured); note that the circuit

parameters are constant across all half-cycles for a given fault current level.

For each half-cycle, there is a total of four arc parameters to be identified: α, β, r, and τ. The parameter r is per definition equivalent to the carbonised path resistance (r_{carb}) because the first order Taylor expansion of (1) around $\mathrm{i_{arc}} = 0\,A$ reduces to $v_{arc} = \mathrm{i_{arc}} \cdot r$. In the following we thus use $\hat{r}_i = r_{carb}$, where the latter is identified for each half-cycle i. We further reduce the number of parameters by choosing $\hat{\tau} = 10\mu s$. We have indeed noticed that the misfit between measured and simulated signals increases for $\tau > 100\mu s$ and is mostly constant for shorter time constants.

The AF parameters α and β remain to be identified. To do so, we first define the error signal

$$e_2(t, i, t_0, \alpha, \beta) = \hat{\sigma}_v^{-1} \cdot \left(\tilde{v}_{arc}(t + t_0) - v_{arc}(t, i)\right)^2 + \hat{\sigma}_i^{-1} \cdot \left(\tilde{\imath}_{arc}(t + t_0) - i_{arc}(t, i)\right)^2, \quad (5)$$

where t_0 is used to synchronise the measured and simulated signals, $\hat{\sigma}_{v,i}$ are the estimated variances of the measured voltage and current (used to normalize current and voltage), $\tilde{v}_{arc}(t)$ and $\tilde{\imath}_{arc}(t)$ are the simulated AF voltage and current signals coming from $\boldsymbol{f_{sim}}(t, \alpha, \beta, \hat{r}_i, \hat{\tau}, \boldsymbol{p_{cir}})$.

For each half-cycle i, the remaining AF parameter alpha and beta are identified by solving the optimization problem

$$\begin{bmatrix}\hat{\alpha}_i \\ \hat{\beta}_i\end{bmatrix} = \arg \min_{\alpha>0, \beta>0, t_0} \int_{t_i}^{t_{i+1}} dt \cdot e_2(t, i, t_0, \alpha, \beta) \quad , \quad (6)$$

Note that the minimisation on t_0 allows to get an optimal time-alignment between measured and simulated signals. The optimisation problem is subsequently solved using a commercial interior-point nonlinear programming solver. To support the convergence to a good minimiser, initial conditions for the AF parameters are set using the simple parameter estimation approach outlined in [8].

In summary, the above procedure yields for each half-cycle i, an estimated arc parameters tuple $\hat{\alpha}_i$, $\hat{\beta}_i$, and $\hat{r}_i$. The error e_2 across all half-cycles of the measured data amounts to approx. 0.3 A_{rms} and 15 V_{rms}.

D. Extraction of physical features from arc fault measurements

In the parameter identification problem (5) we cannot ensure that values of α and β are chosen consistently, i.e. that their values are consistent among different AFs of the same experiment. To address this problem, we segment our measurements in half-cycles and seek for features in AF waveforms, which we refer to as physical features. For later analysis of mathematical parameters, we use the following physical features as a ground truth:

1) Voltage plateau — steady state value reached by the voltage waveform, after the arc has ignited and while the current keeps increasing (Fig. 3), i.e.

$$V_{plateau} := \frac{V_+ + V_-}{2}, \quad (7)$$

2) Voltage asymmetry — ratio between peak values of the voltage signal during the ignition and the extinction of an arc, i.e.

$$V_{asymmetry} := \frac{V_{-,max}}{V_{+,max}}, \quad (8)$$

3) Voltage overshoot — ratio between the average peak voltage and the voltage plateau, i.e.

$$V_{overshoot} := \frac{V_{+\,max} - V_{-\,max}}{V_+ + V_-}, \quad (9)$$

4) Resistance of the carbonized path — ratio of the voltage and current derivatives at zero-crossing that is indicative of the resistance of an AF model when the arc is not ignited, i.e.

$$r_{carb} = \frac{v'}{i'}\Big|_{i=0}. \quad (10)$$

5) Shoulder length –time window between the extinction and ignition of an arc (linear region around zero current).

The methods for extracting the two last features are based on (piecewise) parametric approximation of the current and voltage waveform around current and voltage zeros (Fig. 3).

We observe certain interdependence between the extracted features. For example, Fig. 4a suggests that there is an inversely proportional relation between the voltage plateau and the overshoot of voltage. Furthermore, high voltage overshoot comes with a high voltage asymmetry (Fig. 4b). Fig. 5a reveals that the high voltage overshoot rarely is accompanied by a short period of carbonised path conduction, i.e. a short shoulder length. Fig. 5b shows that the larger the carbonized path resistance the longer the shoulder in the AF waveform. This agrees well with the intuition that a higher resistive path requires higher voltage (power) to ignite the arc.

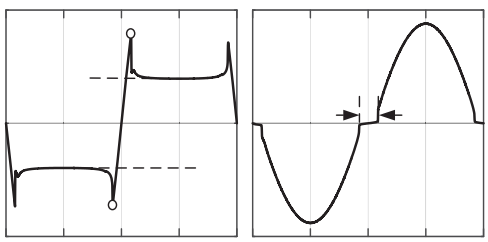

Fig. 3. Values of the arc fault voltage and current that are used to extract physical features.

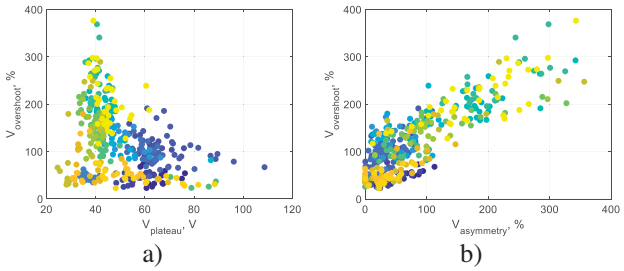

Fig. 4. a) Voltage overshoot as a function of: a) voltage plateau, and b) voltage asymmetry. Each point is a half-cycle of the measured arc fault signal.

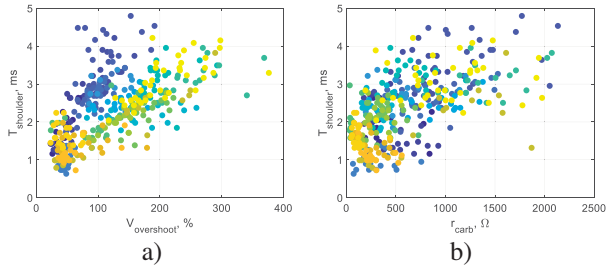

Fig. 5. Shoulder length of arc fault current as a function of: a) voltage overshoot, b) carbonised path resistance. Each point is a half-cycle of the measured arc fault signal.

III. Results

A. Effects of the mathematical arc fault parameters

In this section, we comment the influence of parameters α and β on the simulated arc fault voltage.

Fig. 6a depicts the influence of parameter α on a static characteristic of an AF, which is given by (1-3). Absolute value of the AF voltage increases as the value of the parameter α increases. The transition between the linear region (near zero current) and the asymptote at maximal current is similar for different values of α. In Fig. 6b it is the opposite case: as the value of parameter β changes, the transition between the two regions alters. For higher values of β, the asymptotic behaviour is approached quicker already at lower currents. Furthermore, the difference between the peak voltage and the asymptotic voltage increases as the value of β gets smaller. The fact that β predominantly controls the transition region, while α controls asymptotic voltage indicates that the two parameters mainly control different features of the AF waveform.

Transient simulations in Fig. 7 further show that α and β influence uncorrelated features of the waveform. Parameter α changes the voltage plateau (Fig. 7a) and parameter β influences shoulder duration in current waveform (Fig. 7b) as expected from the analytical expression of the AF static characteristic (1).

B. Relation between physical features and mathematical parameters

To verify if the mathematical structure of the proposed model agrees with empirical evidence, we compare the extracted mathematical parameters against the physical features. The comparison is performed for each half-cycle of the source voltage. Finally, we show Pearson correlation coefficients between all mathematical parameters and physical features (TABLE I).

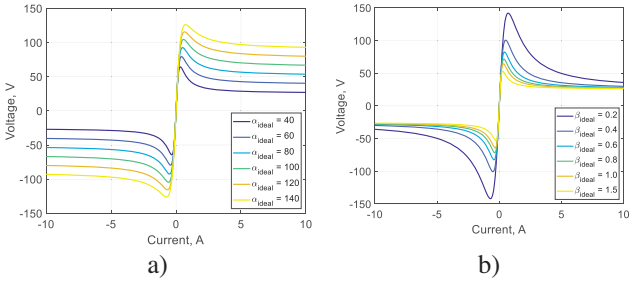

Fig. 6. a) Influence of mathematical parameters a) α and b) β on the static characteristic.

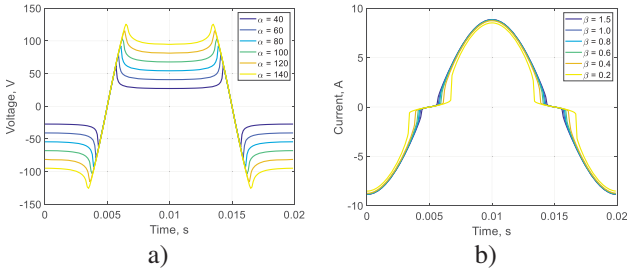

Fig. 7. Transient simulation of arc voltage (a) and current (b). Influence of mathematical parameter: a) α on voltage plateau and b) β on current "shoulders".

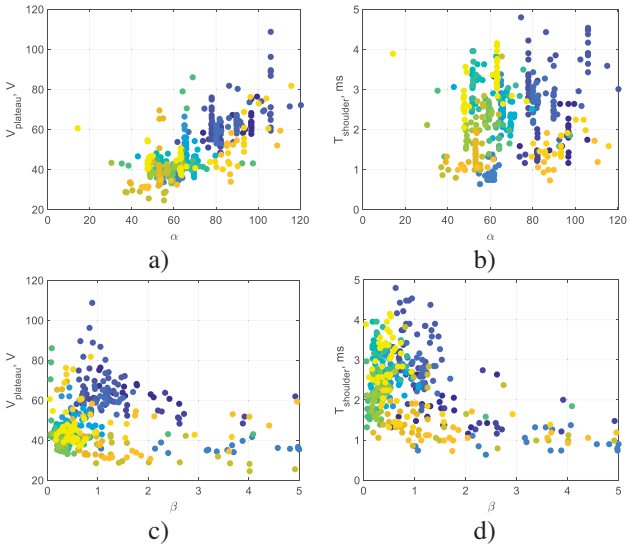

Fig. 8. a) Voltage plateau as a function of parameter α. b) Shoulder length as a function of parameter α. c) Voltage asymmetry as a function of parameter β. d) Shoulder length as a function of parameter β.

Fig. 8a shows a linear relationship between α and the voltage plateau with a correlation of 0.74. Correlation of the parameter β with the voltage plateau is nearly 0 (Fig. 8c). Parameter α shows a low correlation with the shoulder duration $T_{shoulder}$ (Fig. 8b), whereas parameter β shows a correlation of -0.49 with the same feature (Fig. 8d).

To model the AF statistical behavior, the optimal parameter α could be determined solely from the voltage plateau behaviour. On the other hand, the parameter α also contributes to other physical features. Even more so, the parameter β contributes with similar importance to several physical features. For these reasons, we have chosen to model α and β from their empirical statistical distributions as identified from measurements rather than associate them with single physical features.

C. Statistical distribution of the mathematical parameters

We analyse variations in mathematical parameters by investigating their probability density functions.

We first group measurements with the same current level, identify parameters, and split the values of the parameters in 100 bins. Then, we create a histogram for each current level and each parameter: α, β, and *r* (Fig. 9). Parameters β and *r* appear to have a different stochastic distribution for every

TABLE I. PEARSON CORRELATION COEFFICIENTS BETWEEN PHYSICAL FEATURES AND MATHEMATICAL PARAMETERS

Correlation coefficient (Pearson)		Physical features				
		$T_{shoulder}$	$v_{plateau}$	r_{carb}	$v_{overshoot}$	$v_{asymmetry}$
Mathematical parameters	α	0.14703	0.74393	0.16618	-0.34203	-0.39162
	β	-0.49257	-0.071792	-0.02567	-0.47058	-0.40394
	R_c	0.60787	0.18074	1.00000	0.4985	0.3416

[-1.0, -0.7)	[-0.7, -0.5)	[-0.5, -0.3)	[-0.3, -0.1)	[-0.1, +0.1]	(+0.1, +0.3]	(+0.3, +0.5]	(+0.5, +0.7]	(+0.7, +1.0]

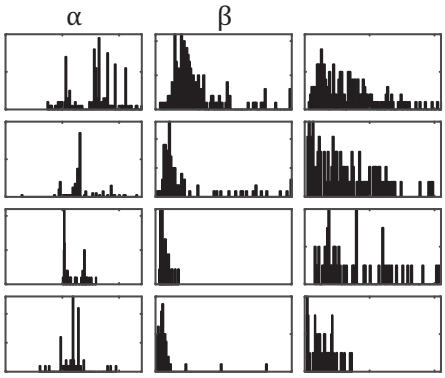

Fig. 9. Histograms of extracted arc parameters for each test current.

current level, whereas parameter α is independent of the current. Furthermore, it is observed that β and r exhibit lognormal distribution for some current levels; See TABLE II. When parameters are not grouped by current levels, neither of the two parameters' distributions is classified as lognormal.

TABLE II. RESULTS OF A χ^2 TEST OF HYPOTHESIS THAT β AND r ARE LOGNORMALLY DISTRIBUTED

	Current level			
	$2.5\ A_{rms}$	$5\ A_{rms}$	$10\ A_{rms}$	$13\ A_{rms}$
β	false	false	true	false
r	true	false	true	false

Extracted histograms are then used to construct a cumulative density function (CDF) of each parameter at each current level. They serve as a base for generating random parameters during transient simulations.

D. Examples of simulation results

Transient simulations of AFs are developed in a VHDL-AMS simulation engine. The mathematical parameters of the AF model are stochastically extracted from their PDF and then fed into the VHDL-AMS model. At each zero-crossing, parameters α and β are altered, while parameter r is altered in the middle of the half-cycle (during the voltage plateau). Parameter r mainly affects the regions before and after the zero-crossing and has little effect once the arc is ignited.

As an example, we generate six tuples of AF parameters for the current level of 10 A_{rms}. We simulate the circuit in Fig. 1 with loads L=7.2 mH and R=17.16 Ω, whose values

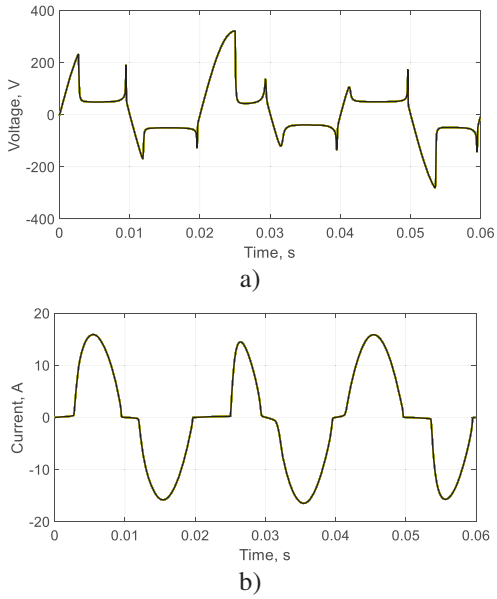

Fig. 10. Simulation of an arc fault at prospective current of 10 A_{rms}: a) voltage, b) current.

are known from arc fault measurements. Fig. 10. shows the output of the transient simulation. The random behaviour of the arc fault is clearly visible.

Another important part of an AF waveform is its high frequency component. We measure the voltage across an arc fault up to 20 MHz and find that the power spectral density decays as K^2/f^k over frequency. We identify these two parameters using a least square fit on the log of the arc fault power spectral density. For different current levels, parameters K and k remain mostly consistent (in our case, K = 15 V and k = 1.58). We build a noise source as a sum of sines with a random phase. Parameters K and k are used to determine the amplitudes of sine waves at given frequencies. The AF noise is modelled as an ideal voltage source (zero impedance) and connected in series with the remaining AF model. Fig. 11 shows the measured power spectral densities of an AF and the power spectral density of the simulated AF. Fig. 12 depicts the simulated time-domain AF noise whose power spectral density is shown in Fig. 11. More precisely, Fig. 12 depicts a 50 µs window at t = 45 ms of the signal in Fig. 10a, where the AF signal is high-pass filtered for illustration purpose (cut-off at 100 kHz to remove the large low frequency component).

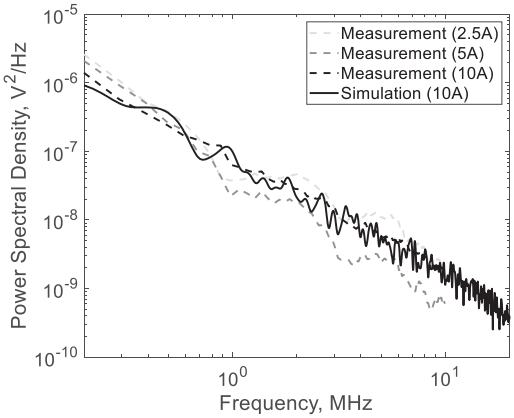

Fig. 11. Power spectrum of high frequency noise during arcing. Arc fault simulations are conducted in VHDL-AMS simulation engine.

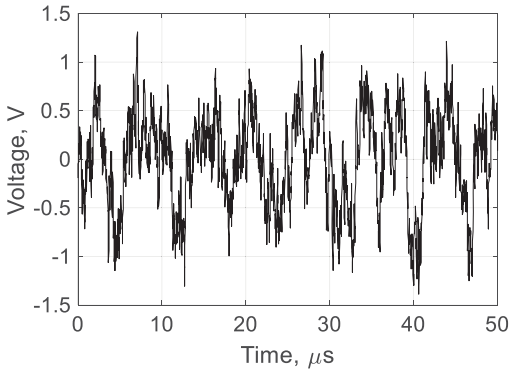

Fig. 12. Transient simulation of arc fault noise. Arc fault simulations are conducted in VHDL-AMS simulation engine.

IV. Discussion

In the analysis of relations between mathematical parameters and physical features there are other relations that have been discovered (TABLE I). For example, overshoots and asymmetry in voltage signal are not only controlled by β as one might expect from looking at the static characteristic (Fig. 6). Correlation between parameter α and those physical features may be explained by looking at the correlation between the voltage plateau (Fig. 4a) and overshoot – α is correlated with the voltage plateau, whereas the voltage plateau is negatively correlated with the voltage overshoot, thus negative correlation between α and the voltage overshoot can be expected.

The fitting error in our parameter identification may come from different sources. First, we change our parameters only after each zero-crossing, therefore we do not account for any variations within the half-cycle of the signal generator. Second, during the optimization of error parameters, α and β might fall into local minima. Third, model parameters have been identified by minimizing the integral error norm (5), which does not necessarily enforce the optimality of parameters in front of other synthetic indicators, such as the physical features.

We find that parameters β and *r* may have a lognormal distribution, but we would need more data to confirm this hypothesis. Richer dataset would also improve the understanding of the stochastic behaviour of α. Furthermore, having a richer dataset could help understand to which extent do arc fault parameters vary once the arc is ignited. In practice, larger variations between arc fault halfwaves (as depicted in Fig. 10) are mostly observed between arc fault waveforms that originate from different test samples.

V. Conclusion

In future work, we will develop models of cables and more complex loads (e.g. drills, dimmers) in VHDL-AMS and use them to simulate realistic scenarios in home installations with AFs. Further open questions include: understanding the evolution of arc fault parameters over time with focus on parameter α, investigating the randomness of AF parameters within a half-wave, and decoupling parameters α and β by modifying the equation of the static characteristic. To address these open questions, we will conduct further measurements of arc faults at current levels between 2.5 A_{rms} and 13 A_{rms} with a finer resolution (e.g. 1 A_{rms}).

In conclusion, we have analysed parameters of a mathematical black-box model by relating them to features of AF measurements. As a result, we reduce the number of free parameters from four to two and establish statistical distributions that determine the randomness of an arc fault as a circuit component. With our proposed parameter identification method, we achieve a fit to measurements with approx. 15 V and 0.3 A RMS error. From high frequency measurements (200 kHz-20 MHz) we confirm the theoretical 1/f shape of arc noise and then use this data to model transient noise. By modelling high frequency behaviour and low frequency stochastic behaviour, we construct a dynamically changing arc fault model for future virtual prototyping applications.

Acknowledgment

We gratefully acknowledge expert advice of Markus Abplanalp on arcing and arc modelling.

References

[1] A. M. Cassie, “Theorie Nouvelle des Arcs de Rupture et de la Rigidité des Circuits,” Cigre, Rep., vol. 102, pp. 588–608, 1939.

[2] O. Mayr, “Beitraege zur Theorie des statischen und des dynamischen Lichtbogens,” Arch. fuer Elektrotechnik, vol. 37, no. 12, pp. 588–608, Dec. 1943.

[3] P. H. Schavemaker and L. Van Der Sluis, “An improved Mayr-type arc model based on current-zero measurements,” IEEE Trans. Power Deliv., vol. 15, no. 2, pp. 580–584, Apr. 2000.

[4] L. R. Orama-Exclusa and B. Rodríguez-medina, “Numerical Arc Model Parameter Extraction for SF6 Circuit Breaker Simulations,” in International Conference on Power Systems Transients, 2003.

[5] U. Habedank, “On the mathematical description of arc behaviour in the vicinity of current zero,” etz. Arch., vol. 10, no. 11, pp. 339–343, 1988.

[6] J. Schwarz, “Dynamisches verhalten eines gasbeblasenen, turbulenzbestimmten schaltlichtbogens,” ETZ-A, vol. 92, no. 3, pp. 389–391, 1971.

[7] W. Rieder and J. Urbanek, New aspects of current-zero research on circuit-breaker reignition. A theory of thermal non-equilibrium arc conditions. na, 1966.

[8] J. Andrea, P. Besdel, O. Zirn, and M. Bournat, “The electric arc as a circuit component,” IECON 2015 - 41st Annu. Conf. IEEE Ind. Electron. Soc., no. February, pp. 3027–3034, 2015.

[9] J. Andrea, M. Bournat, R. Landfried, P. Teste, S. Weber, and P. Schweitzer, “Model of an Electric Arc for Circuit Analysis,” in 28th International Conference on Electric Contacts, 2016, no. June.